Phase Domain of the Cubic *Im*$\bar{3}$*m* Mesoporous Silica in the $EO_{106}PO_{70}EO_{106}$−Butanol−H_2O System

Freddy Kleitz,*,† Tae-Wan Kim,‡ and Ryong Ryoo‡

Department of Chemistry, Université Laval, St Foy, Quebec, G1K 7P4, Canada, and National Creative Research Initiative Center for Functional Nanomaterials, Department of Chemistry (School of Molecular Science-BK21), Korea Advanced Institute of Science and Technology, Daejeon, 305-701 Republic of Korea

Received July 27, 2005. In Final Form: October 27, 2005

n-Butanol has been chosen as an organic additive in the SiO_2−$EO_{106}PO_{70}EO_{106}$−H_2O system at low HCl concentrations, for the generation of large-pore mesoporous silicas with easily tailored textural and structural properties. As opposed to previous reports on syntheses of cubic mesoporous silica that are usually performed in a very narrow composition range, we report now the possibility of preparing large-pore cagelike mesoporous silicas in a wide range of synthesis mixture compositions. Particularly, the cubic *Im*3*m* silica with large interconnected cagelike pores (SBA-16) can easily be synthesized with controlled pore sizes and wall thicknesses, depending upon the synthesis mixture composition. The primary mesopore volume of the SBA-16 cages can be tuned from 0.27 to 0.56 $cm^3\ g^{-1}$, and the mesopore size is shown to range from 4.7 to 7.2 nm, by performing a simple adjustment of the starting mixture composition. With the synthesis parameters varied, we describe the first complete diagram of the product phase domains obtained for silica mesophases in a SiO_2−$EO_{106}PO_{70}EO_{106}$−butanol−H_2O system. Other ordered mesophases also observed in this system are the face-centered cubic *Fm*3*m* silica mesophase and a 2D hexagonal-like mesostructure. Importantly here, the use of a low acid catalyst concentration regime allowed the preparation of silica mesophases in almost thermodynamically controlled conditions because of slow condensation kinetics of the inorganics. Such conditions enabled the introduction of *n*-butanol as the phase-controlling agent in the system, providing efficient tuning of the mesophase topology. The description of the phase domains provides a future basis for the design of large-pore mesoporous silicas with tailored textural and structural properties. Mesoporous samples obtained within the composition ranges of the phase domains are characterized by powder X-ray diffraction (PXRD) and nitrogen physisorption measurements.

Introduction

Ordered mesoporous silicas[1] are attracting wide current interest because of their perspectives as selective sorbents, catalyst supports, matrixes for biomolecules, flow and transport devices, and advanced host−guests systems.[2] In addition, the structure with well-defined porosity makes the silica materials suitable as references for adsorption and diffusion studies. However, practical design of such mesoporous materials requires a high level of understanding of physicochemical factors governing supramolecular assembly at the mesoscale, particularly during the formation of the hybrid inorganic−organic mesophases,[3−6] and detailed knowledge on the relationship between structure and properties. Furthermore, precise control of the structural and textural properties such as pore diameter, pore topology, and pore connectivity is highly desirable to reach ultimately the goal of industrial and commercial applications. In this regard, the use of polyalkylene oxide-based triblock copolymers for the synthesis of mesoporous silicas, such as the pluronic-type triblock copolymers ($EO_nPO_mEO_n$), offers possibilities of tailoring material properties.[7−22] However, most of the large-pore ordered mesoporous silicas are prepared at relatively high acid concentrations around 1.5−2 M, conditions under which the mesophases form through kinetically controlled assembly of the organic and

* To whom correspondence should be addressed. E-mail: freddy.kleitz@chm.ulaval.ca.

† Université Laval.

‡ Korea Advanced Institute of Science and Technology.

(1) (a) Kresge, C. T.; Leonowicz, M. E.; Roth, W. J.; Vartuli, J. C.; Beck, J. S. *Nature* **1992**, *359*, 710. (b) Beck, J. S.; Vartuli, J. C.; Roth, W. J.; Leonowicz, M. E.; Kresge, C. T.; Schmitt, K. D.; Chu, C. T.-W.; Olson, D. H.; Sheppard, E. W.; McCullen, S. B.; Higgins, J. B.; Schenkler, J. L. *J. Am. Chem. Soc.* **1992**, *114*, 10834.

(2) (a) Ciesla, U.; Schüth, F. *Microporous Mesoporous Mater.* **1999**, *27*, 131. (b) Ying, J. Y.; Mehnert, C. P.; Wong, M. S. *Angew. Chem. Int. Ed.* **1999**, *38*, 56. (c) Wirnsberger, G.; Yang, P.; Scott, B. J.; Chmelka, B. F.; Stucky, G. D. *Spectrochim. Acta, Part A* **2001**, *57*, 2049. (d) Schmidt, W.; Schüth, F. *Adv. Mater.* **2002**, *14*, 629. (e) Soler-Illia, G. J. A. A.; Patarin, J.; Lebeau, B.; Sanchez, C. *Chem. Rev.* **2002**, *102*, 4093. (f) Tagushi, A.; Schüth, F. *Microporous Mesoporous Mater.* **2004**, *77*, 1. (g) Hartmann, M. *Chem. Mater.* **2005**, *17*, 4577.

(3) Flodström, K.; Wennerström, H.; Alfredsson, V. *Langmuir* **2004**, *20*, 680.

(4) Flodström, K.; Teixeira, C. V.; Amenitsch, H.; Alfredsson, V.; Lindén, M. *Langmuir* **2004**, *20*, 4885.

(5) Flodström, K.; Wennerström, H.; Teixeira, C. V.; Amenitsch, H.; Lindén, M.; Alfredsson, V. *Langmuir* **2004**, *20*, 10311.

(6) Ruthstein, S.; Frydman, V.; Goldfarb, D. *J. Phys. Chem. B* **2004**, *108*, 9016.

(7) Soler-Illia, G. J. A. A.; Crepaldi, E. L.; Grosso, D.; Sanchez, C. *Curr. Opin. Colloid Interface Sci.* **2003**, *8*, 109 and references therein.

(8) Zhao, D.; Huo, Q.; Feng, J.; Chmelka, B. F.; Stucky, G. D. *J. Am. Chem. Soc.* **1998**, *120*, 6024.

(9) Zhao, D.; Sun, J. Y.; Li, Q. Z.; Stucky, G. D. *Chem. Mater.* **2000**, *12*, 275.

(10) Kim, J. M.; Stucky, G. D. *Chem. Commun.* **2000**, 1159.

(11) Kim, S. S.; Pauly, T. R.; Pinnavaia, T. J. *Chem. Commun.* **2000**, 1661.

(12) Kipkemboi, P.; Fogden, A.; Alfredsson, V.; Flodström, K. *Langmuir* **2001**, *17*, 5398.

(13) Flodström, K.; Alfredsson, V. *Microporous Mesoporous Mater.* **2003**, *59*, 167.

(14) Yu, C.; Tian, B.; Fan, J.; Stucky, G. D.; Zhao, D. *Chem. Commun.* **2001**, 2726.

(15) Liu, X.; Tian, B.; Yu, C.; Gao, F.; Xie, S.; Tu, B.; Che, R.; Peng, L.-M.; Zhao, D. *Angew. Chem. Int. Ed.* **2002**, *41*, 3876.

(16) van der Voort, P.; Benjelloun, M.; Vansant, E. F. *J. Phys. Chem. B* **2002**, *106*, 9027.

(17) Fan, J.; Yu, C.; Gao, F.; Lei, J.; Tian, B.; Wang, L.; Luo, Q.; Tu, B.; Zhou, W.; Zhao, D. *Angew. Chem. Int. Ed.* **2003**, *42*, 3146.

(18) Wang, Y. Q.; Yang, C. M.; Zibrowius, B.; Spliethoff, B.; Lindén, M.; Schüth, F. *Chem. Mater.* **2003**, *15*, 5029.

(19) Matos, J. R.; Kruk, M.; Mercuri, L. P.; Jaroniec, M.; Zhao, L.; Kamiyama, T.; Terasaki, O.; Pinnavaia, T. J.; Liu, Y. *J. Am. Chem. Soc.* **2003**, *125*, 821.

(20) Flodström, K.; Alfredsson, V.; Källrot, N. *J. Am. Chem. Soc.* **2003**, *125*, 4402.

(21) Kruk, M.; Celer, E. B.; Jaroniec, M. *Chem. Mater.* **2004**, *16*, 698.

(22) Kim, T.-W.; Ryoo, R.; Kruk, M.; Gierszal, K. P.; Jaroniec, M.; Kamiya, S.; Terasaki, O. *J. Phys. Chem. B* **2004**, *108*, 11480.

10.1021/la052047+ CCC: $33.50
Published on Web 12/01/2005

inorganic species into nanostructured domains. The rapid mesophase assembly is a limitation for the exact tuning of the textural and structural parameters. Furthermore, mesoporous silicas with cubic symmetry are usually more difficult to prepare than the 2D hexagonal counterparts such as SBA-15, and particularly, cagelike mesophases are often only synthesized in a narrow range of synthesis mixture composition. However, such materials with highly interconnected 3D pore structures are expected to be superior to materials with one-dimensional channels especially for applications dealing with selectively tuned adsorption or diffusion, flow and transport at the nanoscale, and host−guest interactions involving bulky molecules.

In an attempt to improve the system and overcome difficulties connected to uncontrolled mesophase assembly, we recently proposed a strategy based on the combined decrease of the acid concentration and the adjustment of the synthesis mixture composition ratio.[23,24] The low acid concentration enabled us to generate various mesoporous silicas with a satisfying level of textural and structural control in wider synthesis composition ranges. For example, using low HCl concentration regimes, we were able to modify the phase behavior of the silica mesophase, employing *n*-butanol as an additive in the diluted P123−H_2O−HCl system (P123 = $EO_{20}PO_{20}EO_{20}$) to produce large-pore cubic *Ia*$\bar{3}$*d* silica.[25,26] Our investigations demonstrated that the phase behavior of the hybrid silica−copolymer mesophase can be remarkably enriched because of the efficient phase-controlling effect of the polar organic additive, which was enabled by slower silica condensation kinetics.

At a low HCl concentration, butanol was suggested to act preferentially as a cosurfactant agent in the micellar system, providing systematic modification of the mesophase behavior. Therefore, it can be expected that this versatile strategy could be extended for the preparation of other silica mesophases using pluronic F127 ($EO_{106}PO_{70}EO_{106}$) as the structure director in a mixed copolymer−H_2O−BuOH system. Our recent preliminary results suggested that there is indeed a possibility of control of the SiO_2−F127 mesophase structure in the presence of butanol.[27] In the system described, the butanol/triblock copolymer mass ratio only was utilized to direct specifically the formation of high-quality silica mesophases with either cubic *Fm*$\bar{3}$*m*, cubic *Im*$\bar{3}$*m*, or 2D hexagonal structures, with all other synthetic parameters remaining constant. However, the details of the compositional ranges and the physicochemical properties of the mesocage materials were not substantiated, and the syntheses were limited to within a narrow range of conditions. We now report in detail on a complete diagram presenting the synthesis products obtained in the SiO_2−$EO_{106}PO_{70}EO_{106}$−butanol−H_2O system. The diagram presented allows the generation of large-pore cagelike mesostructured silicas with tailored structural features. Emphasis is especially put on the cubic *Im*$\bar{3}$*m* silica (i.e., SBA-16 silica), which could easily be prepared in this $EO_{106}PO_{70}EO_{106}$−butanol−H_2O system with exceptional synthetic tuning of pore size and wall thickness.

Materials and Methods

Materials. The mesostructured silica materials were prepared using a mixture of pluronic F127 (Sigma) and *n*-butanol (Aldrich, 99.4%) as a structure-directing mixture. The silica source was tetraethoxysilane (TEOS, ACROS, 98%). The molar composition of the starting reaction mixture was varied in the range of 0.0035 F127/*x* TEOS/*y* BuOH/0.91 HCl/117 H_2O with $x = \sim 0.5-3$ and $y = \sim 0-3$, respectively. The synthesis procedure is as follows: 5.00 g of pluronic F127 is dissolved in 240 g of distilled water and 10.5 g of hydrochloric acid (35 wt %). After complete dissolution, the selected amount of butanol is added all at once at 45 °C. TEOS is added after 1 h of stirring. The synthesis is carried out in a closed polypropylene bottle. The mixture is further stirred vigorously at 45 °C for 24 h. Subsequently, the mixture is aged at 100 °C for 24 h under static conditions (this process is referred to as hydrothermal treatment). The white precipitated product is then filtered hot without washing and dried at 100 °C for 24 h. In all cases, proper drying should be applied for the high-quality materials before removal of the templating agent. Template-free mesoporous materials are obtained after a brief ethanol/HCl washing, followed by calcination at 550 °C under air.

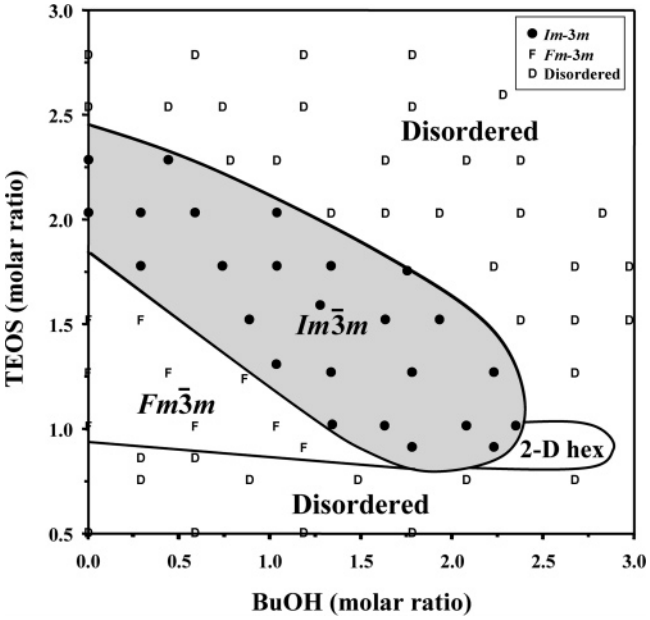

Figure 1. Diagram of mesophase structures established according to the XRD measurements. Each sample is prepared with a molar ratio of 0.0035 F127/*x* TEOS/*y* BuOH/0.91 HCl/117 H_2O. Only some of the samples collected corresponding to phase positions are illustrated on the diagram.

Characterization Methods. X-ray diffraction (XRD) patterns were recorded on a Rigaku Multiplex instrument operated at 1.5 kW, using Cu Kα radiation. High-resolution XRD (HRXRD) data were collected with a powder sample using synchrotron beam line BL8C2 at Pohang Light Source in the reflection mode ($\lambda = 0.154\ 250$ nm). The nitrogen adsorption isotherms were measured at liquid nitrogen temperature (−196 °C) using a Quantachrome Autosorb-1MP volumetric adsorption analyzer. Before the measurements, the silica samples were outgassed under vacuum for 12 h at 300 °C. The Brunauer−Emmett−Teller (BET) equation was used to calculate the surface area from adsorption data obtained at P/P_0 between 0.05 and 0.2. The total volume of micro- and mesopores was calculated from the amount of nitrogen adsorbed at $P/P_0 = 0.95$, assuming that adsorption on the external surface was negligible compared to adsorption in pores. The mesopore diameter is estimated using the non-local density functional theory (NLDFT) method. The model isotherm used for the DFT evaluation was N_2-adsorbed on silica with cylindrical pores using the adsorption branch, which may underestimate systematically the pore size for spherical cagelike geometry.

Results and Discussion

The diagram presenting the phases of synthetic products obtained in the SiO_2−$EO_{106}PO_{70}EO_{106}$−butanol−H_2O system is depicted in Figure 1 as a function of amounts of BuOH and

(23) Choi, M.; Heo, W.; Kleitz, F.; Ryoo, R. *Chem. Commun.* **2003**, 1340.
(24) Kleitz, F.; Liu, D.; Anilkumar, G. M.; Park, I.-S.; Solovyov, L. A.; Shmakov, A. N.; Ryoo, R. *J. Phys. Chem. B* **2003**, *107*, 14296.
(25) Kleitz, F.; Choi, S. H.; Ryoo, R. *Chem. Commun.* **2003**, 2136.
(26) Kim, T.-W.; Kleitz, F.; Paul, B.; Ryoo, R. *J. Am. Chem. Soc.* **2005**, *127*, 7601.
(27) Kleitz, F.; Solovyov, L. A.; Anilkumar, G. M.; Choi, S. H.; Ryoo, R. *Chem. Commun.* **2004**, 1536.

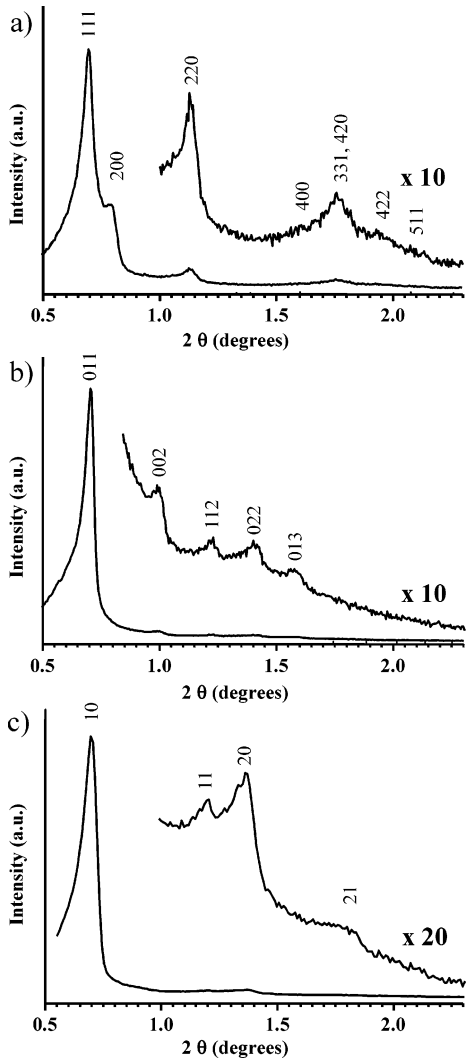

Figure 2. HRXRD patterns of mesoporous silicas synthesized with the composition ratio of 0.0035 F127/x TEOS/y BuOH/0.91 HCl/117 H_2O: (a) $Fm\bar{3}m$ phase with $x = 1.0$, $y = 0$; (b) $Im\bar{3}m$ phase with $x = 1.0$, $y = 1.8$; and (c) $p6mm$ phase with $x = 1.0$, $y = 2.4$.

TEOS present in the starting mixture composition. All mesophases were synthesized at 45 °C followed by subsequent hydrothermal treatment at 100 °C for 24 h, at a fixed HCl concentration of 0.4 M in the aqueous solution. As shown in Figure 1, the use of the $EO_{106}PO_{70}EO_{106}$ copolymer in combination with *n*-butanol as structure-directing mixture for the preparation of mesoporous silica enables the synthesis of silica mesophases with either face-centered cubic (*fcc*) $Fm\bar{3}m$, body-centered cubic (*bcc*) $Im\bar{3}m$, or two-dimensional (2D) hexagonal structures.

The XRD patterns shown in Figure 2 examplify mesostructures obtained with different synthesis mixture compositions. Well-resolved diffraction peaks in the range of $2\theta = 0.6-2.3$ are indexed to the different space groups as indicated, depending upon the BuOH/TEOS ratio in the starting synthesis mixture. At the boundaries of the different mesophase regions, intermediate mixed phases are sometimes observed, indicating small two-phase coexistence regions. In addition, poorly resolved XRD patterns, which could be indexed to no distinct space group, were also obtained and attributed to disordered materials. In the case of materials with the $Fm\bar{3}m$ structure, the well-resolved diffraction pattern with no additional reflections related to the 3D hexagonal (HCP) intergrowths suggests that the cubic phase is obtained in high purity. Notably, the XRD pattern of the $Fm\bar{3}m$ phase exhibits the expected doublet of the (111) and (200) reflections at low 2θ values, characteristic of the $Fm\bar{3}m$ phase (Figure 2a). As we discussed previously, this silica exhibits large cagelike pores arranged in a cubic close-packed mesostructure.[24]

Large phase domains of the diagram of the synthesis products correspond to either the $Im\bar{3}m$ mesophase or disordered materials. Irrespective of the amounts of BuOH added ($0 \le y \le 3.0$), disordered materials are formed for very low values of the TEOS ratio below 0.8−0.9 or high values above 2.4 in molar ratio. These disordered materials have not been further characterized. In the remaining part of the diagram ($0.8 < x < 2.4$), the $Im\bar{3}m$ mesophase is the dominating phase. This silica mesophase is analogous to mesoporous SBA-16 silica, which consists of large spherical cavities arranged in body-centered cubic (*bcc* $Im\bar{3}m$) symmetry.[8,22,28] In the interval of TEOS within $0.9 \le x < 1.75$, a region of $Fm\bar{3}m$ mesophase is visible for low BuOH amounts. In the interval of TEOS within $0.8 < x < 1.0$, the phase behavior is also enriched with the presence of a very small domain of a 2D hexagonal-like phase at high values of BuOH with $y > 2.2$ (Figure 2c).

In the absence of BuOH, the addition of TEOS in the ratio $0.9 \le x \le 1.75$ results in the formation of the $Fm\bar{3}m$ silica mesophase. At a higher TEOS ratio of $1.8 \le x \le 2.4$, the $Im\bar{3}m$ phase is the dominant phase. Therefore, in that case, increasing amounts of TEOS in the system seems to be responsible for the transition from the $Fm\bar{3}m$ phase to the $Im\bar{3}m$ phase. Evidently, the amount of TEOS added to the system greatly influences the nature of the mesophase formed. This fact might be rationalized by pronounced differences in the SiO_2/F127 ratio in the silica−block copolymer hybrid mesophase and the repartition of the inorganic and organic domains. It should also be noted that a significant amount of ethanol is released *in situ* from the hydrolysis of TEOS, leading to possible cosolvent effects[29] perturbating the system. Moreover, at higher TEOS ratios, more silica species are available for the interaction with the polar EO headgroups.

Clearly, the formation of various mesophases is strongly affected not only by the amount of TEOS employed but also by the quantity of BuOH added to the system. In the high TEOS content range ($1.8 \le x \le 2.4$), the addition of butanol first does not change the symmetry of the mesophase ($Im\bar{3}m$), but further addition of butanol provokes the transition from the $Im\bar{3}m$ phase to the disordered phase. The quantity of BuOH needed to induce this transition progressively increases from $y = 0.75$ to as high as $y = 2.25$ with a decreasing amount of TEOS from $x = 2.4$ to 1.8. Evidently, the $Im\bar{3}m$ silica can be prepared in a wider synthesis range if the amount of TEOS employed as the silicon source is reduced accordingly. Furthermore, at the low TEOS content ($0.9 \le x \le 1.8$), the $Im\bar{3}m$ phase is formed uniquely in the presence of a significant amount of butanol. Without BuOH, the $Fm\bar{3}m$ phase remains the dominant phase with $0.9 \le x \le 1.8$. The quantities of BuOH required to induce the phase transition from $Fm\bar{3}m$ to $Im\bar{3}m$ reach values as high as $y = 1.75$, for low TEOS values with x close to 0.9. At this value of TEOS, the addition of amounts of butanol to the starting mixture up to $y = 1.75$ does not alter the symmetry of the mesophase from $Fm\bar{3}m$, but differences in relative intensities of the diffraction peaks are observed (not shown). At $y = 1.75$, the transition to the *bcc* $Im\bar{3}m$ symmetry occurs. A further increase in the amount of butanol added induced the formation of a phase that could be described as "*a near to 2D hexagonal*" SBA-15-type structure.[27] At the fixed TEOS ratio of $x = 0.9$, these structural evolutions

(28) Sakamoto, Y.; Kaneda, M.; Terasaki, O.; Zhao, D.; Kim, J. M.; Stucky, G. D.; Shin, H. J.; Ryoo, R. *Nature* **2000**, *408*, 449.
(29) Ivanova, R.; Lindman, B.; Alexandridis, P. *Adv. Colloid Interface Sci.* **2001**, *89*, 351.

are exclusively due to the addition of different amounts of BuOH as the unique phase-controlling agent.

Butanol is known to act as a cosurfactant,[30−34] most likely comicellizing with the main amphiphilic struture-directing species. In the case of amphiphilic block copolymer−butanol systems, butanol is considered to be located at the interface of the apolar/polar region of the copolymer micelles, permitting variations of the hydrophilic/hydrophobic volume ratios in the aggregates and modulation of their interfacial curvature.[32,35−37] The diagram of the synthesis products obtained for SiO_2 in the F127−BuOH−H_2O system is distinct from classical copolymer−water phase diagrams that describe systems at thermodynamic equilibrium as a function of the concentration of the components. However, we may speculate that the evolution of the mesophase in the F127−BuOH−H_2O system with phase transitions between cagelike *Fm*$\bar{3}$*m* and *Im*$\bar{3}$*m* and the "near-cylindrical" 2D hexagonal pore structure could originate from similar effects based on changes in the hydrophobic/hydrophilic volume fractions and interfacial curvature. It is likely that the curvature of the micellar aggregates could be reduced because of a substantial increase of the apparent apolar volume.[38] These results are very significant because they highlight systematic control over the formation of large-pore mesoporous silica with a tailored pore architecture, by employing structural evolutions induced only by the addition of different amounts of butanol as a mesophase-controlling agent. Such tuning of the mesophase by the addition of organics has been particularly studied by Lindén and co-workers in the cases of various mesostructured materials synthesized with small molecular-weight ionic surfactants.[31,33,39−45] Other authors also reported more recently on the phase control of small-pore mesoporous silica specifically by cosurfactant-assisted syntheses.[46] However, reports on mesophase control with cosurfactant molecules used in block copolymer systems remained rare.[32] Evidently now, the addition of butanol has also emerged as a highly effective method for increasing the phase domains for ordered cagelike mesoporous silicas in the syntheses employing triblock copolymers as structure-directing species.

In contrast to the mesophase behavior of SiO_2 in $EO_{20}PO_{70}EO_{20}$−butanol−H_2O,[27] increasing the amount of the silica source in the F127−BuOH−H_2O system while keeping the BuOH amount constant does not lead to only one possible sequence of phase transitions. The type of transition is highly dependent upon the BuOH content chosen, which is fixed in the starting synthesis mixture. At a low BuOH content ($y \leq 1.5$), increasing the TEOS quantity in the mixture results in a *disorder−fcc−bcc−disorder* transition sequence. At a medium BuOH content ($1.5 < y \leq 2.2$), increasing the amount of TEOS leads to a *disorder−bcc−disorder* sequence. At a high BuOH content ($y > 2.2$), transitions following a *disorder−hexagonal−bcc−disorder* sequence are observed. Finally, a *disorder−hexagonal−disorder* sequence occurs at the highest values of BuOH. Evidently, the silica mesophase behavior is more complex in the $EO_{106}PO_{70}EO_{106}$−BuOH−H_2O system, and therefore, such work may be paving the way for a rich diversity of material textural properties.

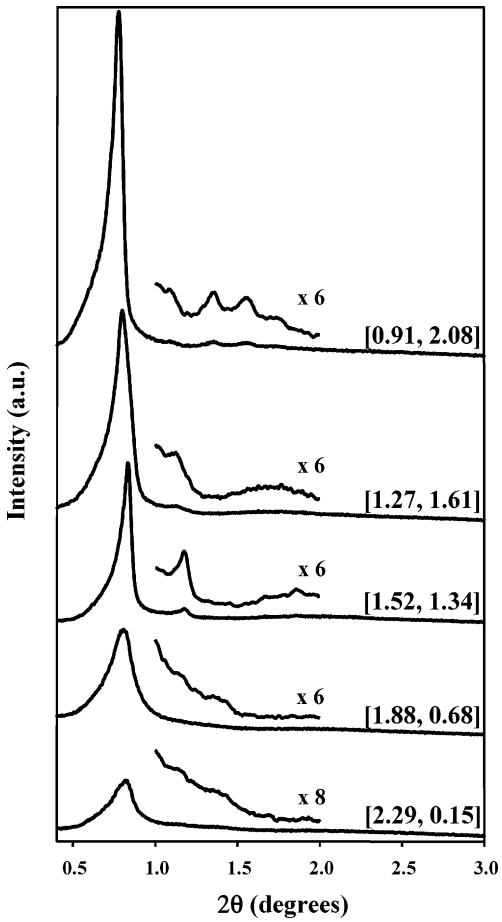

Figure 3. HRXRD patterns for the cubic *Im*$\bar{3}$*m* SBA-16-type mesoporous silicas. Each sample was prepared at the molar ratio of 0.0035 F127/*x* TEOS/*y* BuOH/0.91 HCl/117 H_2O, where (*x*, *y*) was varied as shown.

Especially, our investigations reveal that the structural properties of the cubic *Im*$\bar{3}$*m* mesoporous silicas can be tailored efficiently by simply adjusting the amounts of the silica source and cosurfactant in the synthesis mixture. Figure 3 shows the XRD patterns of mesoporous silica samples obtained in the cubic *Im*$\bar{3}$*m* region of the synthesis product diagram with different values of TEOS and BuOH. All diffraction patterns can be unambiguously indexed to the *Im*$\bar{3}$*m* phase, with, however, clear differences in the position of the diffraction peaks and their relative intensity distributions with changes in the BuOH/TEOS ratio. These changes in the diffraction patterns indicate variations in structural parameters such as unit cell size and, most likely,

(30) Armstrong, J.; Chowdhry, B.; Mitchell, J.; Beezer, A.; Leharne, S. *J. Phys. Chem.* **1996**, *100*, 1738.
(31) Ågren, P.; Lindén, M.; Rosenholm, J. B.; Schwarzenbacher, R.; Kriechbaum, M.; Amenitsch, H.; Laggner, P.; Blanchard, J.; Schüth, F. *J. Phys. Chem. B* **1999**, *103*, 5943.
(32) Feng, P.; Bu, X.; Pine, D. J. *Langmuir* **2000**, *16*, 5304.
(33) Kleitz, F.; Blanchard, J.; Zibrowius, B.; Schüth, F.; Ågren, P.; Lindén, M. *Langmuir* **2002**, *18*, 4963.
(34) Kwon, K.-W.; Park, M. J.; Hwang, J.; Char, K. *Polym. J.* **2001**, *33*, 404.
(35) Holmqvist, P.; Alexandridis, P.; Lindman, B. *Langmuir* **1997**, *13*, 2471.
(36) Holmqvist, P.; Alexandridis, P.; Lindman, B. *Macromolecules* **1997**, *30*, 6788.
(37) Holmqvist, P.; Alexandridis, P.; Lindman, B. *J. Phys. Chem. B* **1998**, *102*, 1149.
(38) Sakya, P.; Seddon, J. M.; Templer, R. H.; Mirkin, R. J.; Tiddy, G. J. T. *Langmuir* **1997**, *13*, 3706.
(39) Lindén, M.; Karlsson, S.; Bussian, P.; Amentisch, H. *Langmuir* **2000**, *16*, 5831.
(40) Ågren, P.; Lindén, M.; Rosenholm, J. B.; Blanchard, J.; Schüth, F.; Amenitsch, H. *Langmuir* **2000**, *16*, 8809.
(41) Lind, A.; Andersson, J.; Karlsson, S.; Ågren, P.; Bussian, P.; Amenitsch, H.; Lindén, M. *Langmuir* **2002**, *18*, 1380.
(42) Tiemann, M.; Goletto, V.; Blum, R.; Babonneau, F.; Amenitsch, H.; Lindén, M. *Langmuir* **2002**, *18*, 10053.
(43) Czuryszkiewicz, T.; Kleitz, F.; Schüth, F.; Lindén, M. *Chem. Mater.* **2003**, *15*, 3704.
(44) Lind, A.; Andersson, J.; Karlsson, S.; Lindén, M.; Rosenholm, J. B. *Colloids Surf., A* **2001**, *183*, 415.
(45) Czuryszkiewicz, T.; Rosenholm, J.; Kleitz, F.; Lindén, M. *Stud. Surf. Sci. Catal.* **2002**, *142*, 1117.
(46) Kao, H.-M.; Cheng, C.-C.; Ting, C.-C.; Hwang, L.-Y. *J. Mater. Chem.* **2005**, *15*, 2989.

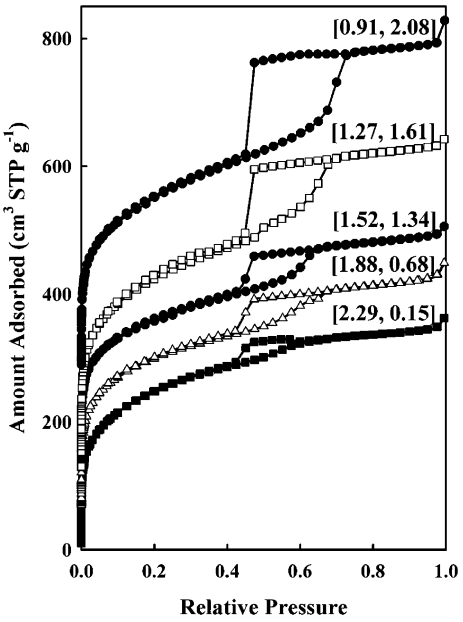

Figure 4. N_2 adsorption−desorption isotherms for cubic $Im\bar{3}m$ silica samples. Each sample was prepared at the molar ratio of 0.0035 F127/*x* TEOS/*y* BuOH/0.91 HCl/117 H_2O, where (*x*, *y*) was varied as shown. The isotherms for (1.88, 0.68), (1.52, 1.34), (1.27, 1.61), and (0.91, 2.08) are offset vertically by 60, 130, 130, and 280 cm^3 g^{-1} STP, respectively.

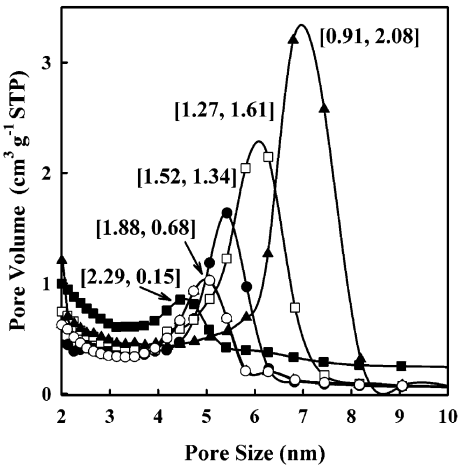

Figure 5. Pore size distributions of the cubic $Im\bar{3}m$ samples (see Figure 4 for compositions). The pore size distribution for the (2.29, 0.15) sample is offset vertically by 0.2 cm^3 g^{-1} STP.

distribution of matter in the unit cell.[47] To further demonstrate that we achieved successful synthetic tuning of cagelike $Im\bar{3}m$ materials, nitrogen physisorption measurements were performed on the different cagelike silicas. The physisorption analyses include the precise measurement of the micropore range. Figures 4 and 5 show the nitrogen adsorption−desorption isotherms and pore size distributions, respectively, for the same series of cubic mesoporous silicas synthesized according to different amounts of BuOH and TEOS in the $Im\bar{3}m$ phase region. The structural parameters of these cubic $Im\bar{3}m$ silica materials are summarized in Table 1. All N_2 isotherms measured are type-IV isotherms with a H2-type adsorption−desorption hysteresis loop characteristic of mesoporous materials with ink-bottle-shaped or cagelike pores.[48,49] Clearly, a pronounced increase of the mesopore volume

(47) Sauer, J.; Marlow, F.; Schüth, F. *Phys. Chem. Chem. Phys.* **2001**, *3*, 1.
(48) Ravikovitch, P. I.; Neimark, A. V. *Langmuir* **2002**, *18*, 1550.
(49) Ravikovitch, P. I.; Neimark, A. V. *Langmuir* **2002**, *18*, 9830.

Table 1. Structural Parameters of the Cubic $Im\bar{3}m$ Mesoporous Silicas That Were Prepared at the Molar Ratio of 0.0035 F127/*x* TEOS/*y* BuOH/0.87 HCl/117 H_2O[a]

(*x*, *y*)	*a* (nm)	S_{BET} (m^2 g^{-1})	S_{ex} (m^2 g^{-1})	V_t (cm^3 g^{-1})	V_{mi} (cm^3 g^{-1})	V_p (cm^3 g^{-1})	w_d (nm)
(2.29, 0.15)	15.3	890	30	0.53	0.22	0.27	4.7
(1.88, 0.68)	15.5	860	40	0.56	0.21	0.30	5.1
(1.52, 1.34)	15.1	810	30	0.56	0.18	0.34	5.4
(1.27, 1.61)	15.6	1050	30	0.77	0.24	0.50	6.3
(0.91, 2.08)	16.2	980	30	0.79	0.19	0.56	7.2

[a] *a* is the XRD unit cell parameter equal to $2^{1/2}d_{110}$; S_{BET} is the apparent BET-specific surface area deduced from the isotherm analysis in the relative pressure range from 0.05 to 0.20; S_{ex} is the external surface area; V_t is total pore volume at a relative pressure of 0.95. V_{mi} and V_p are the micropore volume and primary mesopore volume, respectively, which were estimated from nitrogen adsorption data using the α_s-plot method (Jaroniec, M.; Kruk, M.; Oliver, J. P. *Langmuir* **1999**, *15*, 5410); w_d is the primary mesopore cage diameter estimated using the NLDFT method (the model used for NLDFT evaluation was N_2-adsorbed on silica considering the adsorption branch), see refs 48 and 49.

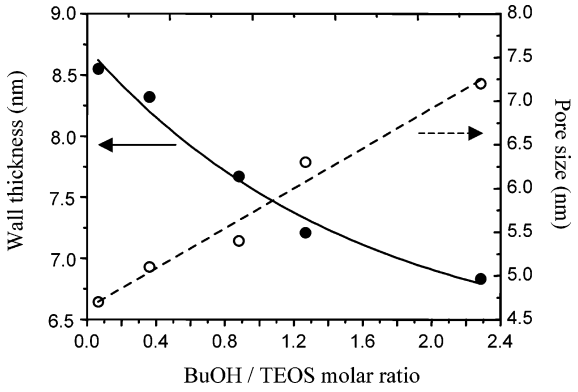

Figure 6. Variation of the wall thickness (●) and pore size (○) of the cubic $Im\bar{3}m$ silica mesophases as a function of the BuOH/TEOS ratio. Minimal wall thicknesses of the *bcc* $Im\bar{3}m$ materials are calculated according to ref 48.

is observed with a simultaneous decrease of the TEOS amount and an increase of the butanol content. Differently, the BET surface areas remain quite comparable for the different samples. The largest mesopore volume and adsorption capacity is measured for the sample synthesized with $x = 0.91$ and $y = 2.08$, whereas the minimum adsorption capacity is measured for $x = 2.29$ and low amounts of butanol ($y = 0.15$). This behavior is also reflected on the dimension of the cages as illustrated by the evolution of the pore size distribution (Figure 5). The main mesopore diameter is estimated by the NLDFT method, using the model isotherm of N_2 adsorbed on silica with cylindrical pores, which may underestimate slightly the pore size for the spherical cagelike geometry. The mesopore volume of the SBA-16 cages is evolving from 0.27 to 0.56 cm^3 g^{-1}, and the diameter of the mesoporous cages is shown to range from 4.7 to 7.2 nm, with a simple adjustment of the starting mixture composition. This relationship between pore dimensions and synthesis composition is comparable to that observed for large-pore cubic $Ia\bar{3}d$ silicas.[26] Plots of the wall thickness and mesopore size as a function of the BuOH/TEOS ratio employed for the mesostructured silica syntheses are shown in Figure 6. As it can be seen, the pore size increases monotonically with a concurrent increase of butanol and a decrease of the quantity of the silica source. However, the wall thickness, as evaluated by a geometrical model proposed by Ravikovitch and Neimark,[48] is shown to decrease noticeably as a function of the increasing BuOH/TEOS ratio. This could be rationalized by the fact that the location of butanol at the hydrophilic−hydrophobic interface may contribute to a shift of

the silica region in the micelles. Hence, in combination with lower amounts of silica species available, the presence of butanol may result in reducing the silica wall thickness. On the other hand, syntheses involving large amounts of TEOS lead to cubic *Im*$\bar{3}$*m* silica materials with thick walls and relatively small mesopore cages. Such a facile synthetic control of pore size and pore wall thickness is a significant advance in the synthesis of cagelike SBA-16-type materials with tailored textural properties and may be further combined with other methods such as aging and thermal treatments.[22] In addition, the thus-prepared materials could become versatile hard templates for the *nanocasting* preparation[50−53] of nonsiliceous mesoporous materials with easily tunable pore sizes.

Conclusions

The synthesis route associating pluronic F127 triblock copolymer and *n*-butanol as a structure-directing mixture is shown to be a very effective method for increasing the phase domains for ordered cagelike mesoporous silicas with cubic *Im*$\bar{3}$*m* or *Fm*$\bar{3}$*m* symmetry. The extended phase domains allow facile synthesis of the large-pore mesoporous silicas with a wider variety of structural and physicochemical properties (i.e., tunable pore diameters, wall thickness, etc.). Importantly, we demonstrated that the cubic *Im*$\bar{3}$*m* SBA-16-type silica can easily be synthesized in a wide range of reactant compositions in the $SiO_2-EO_{106}-PO_{70}EO_{106}-BuOH-H_2O$ system. Highly ordered 3D cubic *Im*$\bar{3}$*m* silicas with tailored pore size and wall thickness could be produced by adjusting the BuOH/TEOS ratio in the synthesis starting mixture. It should be emphasized that such a straightforward tailoring of the mesophase behavior was made possible because of the low concentration of the acid catalyst (HCl). Butanol is an additive of choice in our system because it is an easily accessible and cheap cosurfactant molecule that enables particularly efficient and reproducible tuning of the mesophase behavior. It would now be tempting to pay our attention to the development of such synthesis strategies by using other organic additives, which might provide future bases for the design of large-pore mesoporous materials and their applications. With this perspective, however, it is important to keep in mind not to diminish the significant advantages that we have gained with the use of butanol by searching for other systems that might sometimes be less applicable.

Acknowledgment. F. K. thanks the Canadian Government for the Canada Research Chair in Functional Nanostructured Materials (2005−2010). The work was supported by the Korea Ministry of Science and Technology and the School of Molecular Science through the Brain Korea 21 project. Synchrotron radiation XRD experiments at PLS were supported in part by MOST and POSTECH.

LA052047+

(50) Ryoo, R.; Joo, S. H.; Kruk, M.; Jaroniec, M. *Adv. Mater.* **2001**, *13*, 677.
(51) Kim, T.-W.; Ryoo, R.; Gierszal, K. P.; Jaroniec, M.; Solovyov, L. A.; Sakamoto, Y.; Terasaki, O. *J. Mater. Chem.* **2005**, *15*, 1560.
(52) Schüth, F. *Angew. Chem. Int. Ed.* **2003**, *42*, 3604.
(53) Feng, H. F.; Zhao, D. Y. *J. Mater. Chem.* **2005**, *15*, 1217.